

Performance Analysis of Digital Beamforming mmWave MIMO with Low-Resolution DACs/ADCs

Faruk Pasic*, Mariam Mussbah*†, Stefan Schwarz*, Markus Rupp*, Fredrik Tufvesson†,
and Christoph F. Mecklenbräuker*

*Institute of Telecommunications, TU Wien, Vienna, Austria

†Christian Doppler Laboratory for Digital Twin assisted AI for sustainable Radio Access Networks

‡Department of Electrical and Information Technology, Lund University, Lund, Sweden

faruk.pasic@tuwien.ac.at

Abstract—Future wireless communications will rely on multiple-input multiple-output (MIMO) beamforming operating at millimeter wave (mmWave) frequency bands to deliver high data rates. To support flexible spatial processing and meet the demands of latency-critical applications, it is essential to use fully digital mmWave MIMO beamforming, which relies on accurate channel estimation. However, ensuring power efficiency in fully digital mmWave MIMO systems requires the use of low-resolution digital-to-analog converters (DACs) and analog-to-digital converters (ADCs). The reduced resolution of these quantizers introduces distortion in both transmitted and received signals, ultimately degrading system performance. In this paper, we investigate the channel estimation performance of mmWave MIMO systems employing fully digital beamforming with low-resolution quantization, under practical system constraints. We evaluate the system performance in terms of spectral efficiency (SE) and energy efficiency (EE). Simulation results demonstrate that a moderate quantization resolutions of 4-bit per DAC/ADC offers a favorable trade-off between energy consumption and achievable data rate.

Index Terms—mmWave, MIMO, channel estimation, digital beamforming, quantization.

I. INTRODUCTION

Millimeter wave (mmWave) communication systems combined with multiple-input multiple-output (MIMO) techniques offer the potential to meet growing data rate demands [1], [2]. To fully exploit the spatial multiplexing and beamforming capabilities of MIMO, fully digital beamforming architectures are required. These architectures enable simultaneous channel estimation in multiple spatial directions within a single time interval, significantly reducing the time overhead for link establishment and making them particularly well-suited for latency-critical applications [3].

Nevertheless, compared to power-efficient analog or hybrid beamforming architectures, fully digital beamforming in wideband mmWave systems tends to be significantly more power-intensive. This is primarily due to the fact that each radio frequency (RF) chain requires a dedicated pair of digital-to-analog converters (DACs) at the transmitter and analog-to-digital converters (ADCs) at the receiver. To reduce power

The work of F. Pasic has been supported by TU Wien with a KuWi Scholarship. The work of M. Mussbah has been funded by the Christian Doppler Laboratory for Digital Twin assisted AI for sustainable Radio Access Networks, Institute of Telecommunications, TU Wien.

consumption, fully digital beamformers must utilize low-resolution converters [4], which in turn introduce distortion in both the transmitted and received signals. Therefore, it is essential to evaluate the performance of such systems under practical hardware constraints.

The performance of digital mmWave beamforming systems employing low-resolution quantizers has been explored to some extent in the literature [5]–[7]. However, these studies are limited in terms of the range of antenna configurations and/or the channel conditions considered. Moreover, to the best of the author’s knowledge, the effect of low-resolution quantization on advanced mmWave MIMO channel estimation techniques remains unexplored.

Contribution: In this paper, we evaluate the performance of fully digital low-resolution mmWave MIMO systems for various channel estimation methods. Our analysis considers different antenna configurations and varying channel conditions characterized by the Rician K -factor. We investigate the impact of reduced quantization resolution through simulations in terms of spectral efficiency (SE) and energy efficiency (EE).

Organization: Section II describes the system model along with the adopted quantization noise model. A simulation-based performance evaluation is presented in Section III, and Section IV concludes the paper.

Notation: We use x to denote scalars, \mathbf{x} for vectors (bold lowercase), and \mathbf{X} for matrices (bold uppercase). The j -th column of a matrix \mathbf{X} is denoted by $\mathbf{X}_{:,j}$. Transpose and Hermitian transpose operations are denoted by $(\cdot)^T$ and $(\cdot)^H$, respectively. The Euclidean norm is written as $\|\cdot\|$, the Frobenius norm as $\|\cdot\|_F$ and the expectation operator as $\mathbb{E}(\cdot)$.

II. SYSTEM MODEL

We study a point-to-point mmWave MIMO system operating in the radiative far-field, assuming perfect synchronization between the transmitter and receiver. The transmitter is equipped with M_{Tx} and the receiver with M_{Rx} antenna elements. Each antenna is equipped with its own RF chain, enabling fully digital beamforming. The system employs time-division duplex (TDD) to ensure channel reciprocity. Additionally, the system utilizes orthogonal frequency-division multiplexing (OFDM) and quadrature amplitude modulation with N subcarriers.

At the n -th OFDM subcarrier, the channel matrix is denoted as $\mathbf{H}[n] \in \mathbb{C}^{M_{\text{Rx}} \times M_{\text{Tx}}}$, based on the equivalent complex baseband representation. The channel is modeled as a frequency-selective Rician fading channel based on the 3rd Generation Partnership Project (3GPP) MIMO channel model, with an adjustable Rician K -factor [8].

A. Link Establishment

Link establishment consists of two phases: training and data transmission. During the training phase, the wireless channel is estimated and the resulting channel estimate is used in the subsequent data transmission phase.

1) *Training Phase*: In the training phase, known pilot symbols are transmitted. The input-output relationship is given by

$$\mathbf{y}[n] = \mathbf{H}[n] (\phi[n] + \mathbf{d}[n]) + \mathbf{w}[n], \quad (1)$$

where $\mathbf{y}[n] \in \mathbb{C}^{M_{\text{Rx}} \times 1}$ represents the unquantized received symbols, $\phi[n] \in \mathbb{C}^{M_{\text{Tx}} \times 1}$ represents the transmitted pilot symbols, $\mathbf{d}[n] \in \mathcal{CN}(0, \sigma_d^2 \mathbf{I}_{M_{\text{Tx}}})$ models impairments from the entire transmit chain as in [9], and $\mathbf{w}[n] \in \mathcal{CN}(0, \sigma_w^2 \mathbf{I}_{M_{\text{Rx}}})$ is the additive white Gaussian noise (AWGN). The pilot symbols for the t -th transmit antenna are defined as

$$\phi_t[n] = \begin{cases} \phi[n], & n \in \{t, t + M_{\text{Tx}}, \dots, N - M_{\text{Tx}} + t\} \\ 0, & \text{else} \end{cases} \quad (2)$$

where $\phi[n]$ are one-dimensional complex symbols drawn from a quadrature amplitude modulation (QAM) alphabet. The transmitter impairments include RF impairments (such as those from the power amplifier (PA) and local oscillator (LO) phase noise) with a combined power denoted by σ_{RF}^2 , as well as quantization noise from DAC with power $\sigma_{q,\text{Tx}}^2$ [9]. To model the effect of low-resolution quantization, we adopt the additive quantization noise model (AQNM), following the approach used in [6], [10]. Adopting this model, the power of the quantization noise from the DAC is given by

$$\sigma_{q,\text{Tx}}^2 = \frac{1}{M_{\text{Tx}}} \Upsilon(n_b) (1 - \Upsilon(n_b)), \quad (3)$$

with the inverse coding gain approximated by $\Upsilon(n_b) \approx \frac{\pi\sqrt{3}}{2} n_b^{-2}$ [11], where n_b denotes the number of quantization bits and $\Upsilon(n_b) = 0$ corresponds to the ideal case of infinite quantization resolution. Therefore, the total impairment power is given by $\sigma_d^2 = \sigma_{\text{RF}}^2 + \sigma_{q,\text{Tx}}^2$. Since both $\mathbf{d}[n]$ and $\mathbf{w}[n]$ are mutually independent and Gaussian, they can be combined into a single noise term, we can rewrite (1) as

$$\mathbf{y}[n] = \mathbf{H}[n] \phi[n] + \mathbf{w}'[n], \quad (4)$$

with $\mathbf{w}'[n] \in \mathcal{CN}(0, \sigma_w^2 \mathbf{I}_{M_{\text{Rx}}} + \sigma_d^2 \mathbf{R}_H)$ and the channel correlation matrix given by $\mathbf{R}_H = \mathbb{E}(\mathbf{H}[n] (\mathbf{H}[n])^H)$. At the receiver, the channel estimate $\tilde{\mathbf{H}}[n] \in \mathbb{C}^{M_{\text{Rx}} \times M_{\text{Tx}}}$ is obtained via least-squares (LS) estimation followed by linear interpolation from the quantized received symbols $\mathbf{y}_q[n]$. The quantized symbols are obtained by adding the quantization noise from the ADC, following the AQNM from [6], [10]

$$\mathbf{y}_q[n] = (1 - \Upsilon(n_b)) \mathbf{y}[n] + \mathbf{w}_q[n], \quad (5)$$

where $\mathbf{w}_q[n] \in \mathcal{CN}(0, \sigma_{q,\text{Rx}}^2 \mathbf{I}_{M_{\text{Rx}}})$ is the quantization noise from the ADC with the power given by

$$\sigma_{q,\text{Rx}}^2 = \Upsilon(n_b) (1 - \Upsilon(n_b)) \mathbb{E}(\|\mathbf{y}[n]\|_2^2), \quad (6)$$

assuming that $\mathbb{E}(\|\mathbf{y}[n]\|_2^2) = 1 + \sigma_w^2$. To enable optimal beamforming, the estimated channel at the receiver must also be available at the transmitter. Since the system operates under a TDD protocol, we leverage channel reciprocity to ensure the transmitter has access to the same channel estimate.

2) *Data Transmission*: The channel estimate obtained in the training phase is processed according to the advanced channel estimation methods described in [12], [13]. The resulting channel estimate $\bar{\mathbf{H}}[n]$ is then used for precoding and combining. To obtain optimal performance in terms of SE, we apply singular value decomposition (SVD) to $\bar{\mathbf{H}}[n]$, with its compact form denoted by

$$\bar{\mathbf{H}}[n] = \bar{\mathbf{Q}}[n] \bar{\Sigma}[n] (\bar{\mathbf{F}}[n])^H. \quad (7)$$

In (7), $\bar{\mathbf{Q}}[n] \in \mathbb{C}^{M_{\text{Rx}} \times \ell_{\text{max}}}$ contains left singular vectors, $\bar{\mathbf{F}}[n] \in \mathbb{C}^{M_{\text{Tx}} \times \ell_{\text{max}}}$ contains right singular vectors, $\bar{\Sigma}[n]$ is the diagonal matrix of singular values $\bar{\sigma}_{(1)}[n], \dots, \bar{\sigma}_{(\ell_{\text{max}})}[n]$ and $\ell_{\text{max}} = \min(M_{\text{Rx}}, M_{\text{Tx}})$ denotes the maximum number of spatial streams. The power loading matrix $\bar{\mathbf{P}}[n] = \text{diag}(\bar{p}_{(1)}[n], \dots, \bar{p}_{(\ell_{\text{max}})}[n])$ is optimized via the water-filling algorithm to maximize the transmission rate, while ensuring compliance with the total transmit power constraint

$$\left\| \bar{\mathbf{F}}[n] (\bar{\mathbf{P}}[n])^{1/2} \right\|_F^2 = P_{\text{T}}. \quad (8)$$

The input-output relationship for data transmission is given by

$$\mathbf{y}[n] = (\bar{\mathbf{Q}}[n])^H \bar{\mathbf{H}}[n] \bar{\mathbf{x}}[n] + (\bar{\mathbf{Q}}[n])^H \mathbf{w}[n], \quad (9)$$

where $\bar{\mathbf{x}}[n]$ represents the precoded transmit symbols including transmitter impairments $\mathbf{d}[n]$

$$\bar{\mathbf{x}}[n] = \bar{\mathbf{F}}[n] (\bar{\mathbf{P}}[n])^{1/2} \mathbf{x}[n] + \mathbf{d}[n], \quad (10)$$

$\mathbf{x}[n] \in \mathbb{C}^{\ell_{\text{max}} \times 1}$ is the transmit symbol vector, $\mathbf{y}[n] \in \mathbb{C}^{\ell_{\text{max}} \times 1}$ is the unquantized received symbol vector and $\mathbf{w}[n] \in \mathcal{CN}(0, \sigma_w^2 \mathbf{I}_{M_{\text{Rx}}})$ is the AWGN. As in (1), we rewrite (9) as

$$\mathbf{y}[n] = (\bar{\mathbf{Q}}[n])^H \bar{\mathbf{H}}[n] \bar{\mathbf{F}}[n] (\bar{\mathbf{P}}[n])^{1/2} \mathbf{x}[n] + (\bar{\mathbf{Q}}[n])^H \mathbf{w}'[n]. \quad (11)$$

Finally, the quantized received symbols are given by $\bar{\mathbf{y}}_q[n]$, following the approach as in (5).

B. Power Consumption Model

To account for the power efficiency of the converters, as well as other key components within the RF chains that significantly contribute to the overall power consumption, we model the total power consumption of our MIMO transceiver as $P_{\text{tot}} = P_{\text{Tx}} + P_{\text{Rx}}$, where P_{Tx} and P_{Rx} denote the transmitter and receiver power consumptions, respectively. The transmitter chain consists of DACs, mixers and PAs. The total transmit power consumption is modeled as [6]

$$P_{\text{Tx}} [\text{mW}] = M_{\text{Tx}} (P_{\text{DC,PA}} + P_{\text{LO}} + 2P_{\text{DAC}}), \quad (12)$$

TABLE I
SIMULATION PARAMETERS

Parameter	Value
Carrier Frequency f_c	25.5 GHz
Bandwidth B	403.2 MHz
Subcarrier Spacing Δf	120 kHz
Sampling Rate f_s	806.4 MHz
RF Impairments Power σ_{RF}^2	-25 dB [7]
Mixer P_{LO} / IL_{mix}	10 dBm / 6 dB [9]
EIRP / PA Power Added Eff. η_{PA}	30 dBm / 20%
LNA Power Cons. $P_{DC,LNA}$	11 mW [14]
Fig. of Merit FoM_{DAC} / FoM_{ADC}	65 fJ/conv / 67.6 fJ/conv [6]
ADC/DAC Resolution Bits n_b	{2, 4, 8}

where $P_{DC,PA}$ is the DC power consumption of the PA, P_{LO} is the power consumption of the mixer (driven by the LO), and P_{DAC} denotes the power consumed by one DAC. To achieve a desired effective isotropic radiated power (EIRP), the output power per PA is given by

$$P_{out,PA} [\text{dBm}] = \text{EIRP} - 20 \log_{10} (M_{Tx}) \quad (13)$$

and the corresponding DC power drawn by the PA is modeled as [6]

$$P_{DC,PA} [\text{mW}] = \frac{1}{\eta_{PA}} \left(10^{\frac{P_{out,PA}}{10}} - 10^{\frac{P_{in,PA}}{10}} \right), \quad (14)$$

where η_{PA} is the power added efficiency of the PA, and $P_{in,PA}$ is the input power to the PA (in dBm). The input power to the PA is given by

$$P_{in,PA} [\text{dBm}] = P_{in,BB} - 10 \log_{10} (M_{Tx}) - IL_{mix}, \quad (15)$$

where $P_{in,BB}$ is the power delivered by the baseband circuitry and IL_{mix} is insertion loss (IL) of the mixer. The power consumption of the DAC is modeled as a function of its resolution n_b (in bits) and sampling rate f_s , and is given by [6]

$$P_{DAC} [\text{mW}] = 2^{n_b} f_s FoM_{DAC}, \quad (16)$$

where FoM_{DAC} denotes the figure of merit of the DAC, typically expressed in femtojoules per conversion step.

The receiver chain consists of low noise amplifiers (LNAs), mixers, and ADCs. The total receiver consumption is given by [6]

$$P_{Rx} [\text{mW}] = M_{Rx} (P_{DC,LNA} + P_{LO} + 2P_{ADC}) \quad (17)$$

where $P_{DC,LNA}$ is the DC power consumption of the LNA and P_{ADC} denotes the power consumed by one ADC. The power consumption of the ADC is modeled as a function of its resolution n_b (in bits) and sampling rate f_s , and is given by [6]

$$P_{ADC} [\text{mW}] = 2^{n_b} f_s FoM_{ADC}, \quad (18)$$

where FoM_{ADC} represents the figure of merit of the ADC.

III. SIMULATION-BASED COMPARISON

To evaluate the system performance, we simulate the SE and EE in a frequency-selective channel. The transmitter and receiver antenna elements are arranged in a uniform linear array (ULA) configuration with half-wavelength spacing. The channel model follows the 3GPP urban macro for the line-of-sight (LOS) scenario with an adjustable K -factor (as outlined in [8]) and the used simulation parameters are summarized in Tab. I. As advanced channel estimation methods, we employ the OOBA-MRC method proposed in [12] and the orthogonal matching pursuit (OMP) method detailed in [13]. In addition to the advanced methods, we also include the performance of conventional baseline method, where the channel estimates is set as $\bar{\mathbf{H}}[n] = \tilde{\mathbf{H}}[n]$. The achievable SE expressed in bits/s/Hz is defined as

$$SE = \frac{1}{N} \sum_{n=1}^N \sum_{\mu=1}^{\ell_{\max}} \log_2 (1 + \text{SINR}_{\mu}[n]), \quad (19)$$

where the effective signal-to-interference-and-noise ratio (SINR) for the spatial stream μ is given by [12]

$$\text{SINR}_{\mu}[n] = \frac{|\bar{\mathbf{G}}_{\mu,\mu}[n]|^2}{\sum_{\substack{\nu=1 \\ \nu \neq \mu}}^{\ell_{\max}} |\bar{\mathbf{G}}_{\mu,\nu}[n]|^2 + \sigma_{\text{tot}}^2[n] \|\bar{\mathbf{Q}}_{:, \mu}[n]\|^2}, \quad (20)$$

with $\sigma_{\text{tot}}^2[n] = \sigma_{\mu}^2[n] + \sigma_w^2 + \sigma_d^2 + \sigma_{q,Rx}^2$. In (20), the term $\bar{\mathbf{G}}_{\mu,\nu}[n]$, where $\mu, \nu \in \{1, \dots, \ell_{\max}\}$, denotes the entries of the channel gain matrix $\bar{\mathbf{G}}[n] \in \mathbb{C}^{\ell_{\max} \times \ell_{\max}}$ for subcarrier n , defined as

$$\bar{\mathbf{G}}[n] = (\bar{\mathbf{Q}}[n])^H \bar{\mathbf{H}}[n] \bar{\mathbf{F}}[n] (\bar{\mathbf{P}}[n])^{1/2}. \quad (21)$$

Furthermore, $\sigma_{\mu}^2[n]$ represents the diagonal entries (variances) of the estimation error covariance matrix $\bar{\mathbf{C}}_{\varepsilon}[n] = \frac{1}{\ell_{\max}} \bar{\varepsilon}[n] (\bar{\varepsilon}[n])^H$. The error $\bar{\varepsilon}[n]$ represents the difference between the channel gain matrix computed using the estimated precoder/combiner $\bar{\mathbf{G}}[n]$, and that obtained using the ideal precoder/combiner $\mathbf{G}[n]$. The achievable EE, expressed in bits/s/Hz/W, is defined by $EE = SE/P_{\text{tot}}$ [7].

We analyze the impact of varying antenna configurations on system performance, with the results in terms of SE and EE shown in Fig. 1 for an SNR of 0 dB. It can be observed that SE mainly increases while EE decreases with the number of antennas, regardless of the employed channel estimation method or the considered K -factor. Furthermore, the achievable SE decreases with lower DAC/ADC resolution.

Results at K-factor of -20 dB: All methods exhibit comparable performance in terms of SE, with the OMP method showing slightly improved performance as the number of antennas increases. The highest EE is achieved with 4-bit quantizer resolution across all channel estimation methods. Notably, the conventional and OMP methods exhibit higher EE than the OOBA-MRC method, which requires the support of the sub-6 GHz MIMO system to achieve comparable SE.

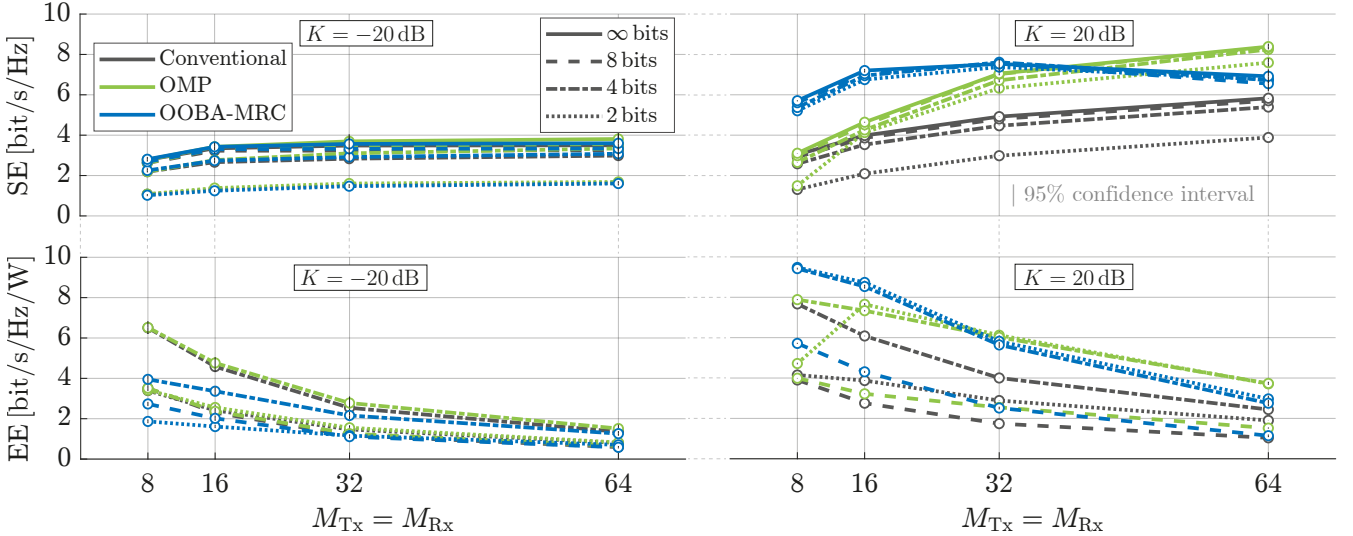


Fig. 1. With a low K -factor (left), lower resolution reduces SE for all methods, while 4-bit quantization yields the highest EE. At high K -factor (right), the OOBA-MRC is more robust to quantization, with 2-bit and 4-bit quantizers achieving high SE and EE.

Results at K-factor of 20 dB: In terms of SE, the OOBA-MRC method consistently outperforms the conventional method across all MIMO configurations, and exceeds the OMP method for 8×8 , 16×16 , and 32×32 configurations. For 64×64 , however, OMP achieves higher SE due to resolution mismatch between the sub-6 GHz (8×8) and mmWave arrays, which degrades OOBA-MRC performance. The conventional method suffers noticeable SE loss at lower quantizer resolutions, while OOBA-MRC and OMP remain more robust. In terms of EE, the conventional method achieves its best performance with a 4-bit quantizer, while the OOBA-MRC and OMP methods attain comparable peak performance using either 2-bit and 4-bit quantizers. The strong LOS component enables reliable estimation even at 2-bit resolution. Additionally, both advanced methods outperform the conventional method in terms of EE across all MIMO configurations.

IV. CONCLUSION

Reducing the quantizer resolution generally leads to a degradation in SE. However, using 4-bit quantizers provides the highest EE, thereby offering a favorable trade-off between power consumption and achievable data rate. At low K -factors, all channel estimation methods experience a decline in SE as the quantizer resolution is reduced. At higher K -factors, although conventional and OMP methods experience performance degradation, the OOBA-MRC method remains robust and largely unaffected in terms of SE.

REFERENCES

- [1] A. F. Molisch, C. F. Mecklenbräuker, T. Zemen, A. Prokes, M. Hofer, F. Pasic, and H. Hammoud, “Millimeter-wave V2X channel measurements in urban environments,” *IEEE Open Journal of Vehicular Technology*, vol. 6, pp. 520–541, 2025.
- [2] F. Pasic, N. Di Cicco, M. Skocaj, M. Tornatore, S. Schwarz, C. F. Mecklenbräuker, and V. Degli-Esposti, “Multi-band measurements for deep learning-based dynamic channel prediction and simulation,” *IEEE Communications Magazine*, vol. 61, no. 9, pp. 98–104, 2023.
- [3] C. Liu, M. Li, L. Zhao, P. Whiting, S. V. Hanly, and I. B. Collings, “Millimeter-Wave Beam Search With Iterative Deactivation and Beam Shifting,” *IEEE Transactions on Wireless Communications*, vol. 19, no. 8, pp. 5117–5131, 2020.
- [4] J. Singh, O. Dabber, and U. Madhow, “On the limits of communication with low-precision analog-to-digital conversion at the receiver,” *IEEE Transactions on Communications*, vol. 57, no. 12, pp. 3629–3639, 2009.
- [5] L. N. Ribeiro, S. Schwarz, M. Rupp, and A. L. F. de Almeida, “Energy efficiency of mmWave massive MIMO precoding with low-resolution DACs,” *IEEE Journal of Selected Topics in Signal Processing*, vol. 12, no. 2, pp. 298–312, 2018.
- [6] S. Dutta, C. N. Barati, D. Ramirez, A. Dhananjay, J. F. Buckwalter, and S. Rangan, “A Case for Digital Beamforming at mmWave,” *IEEE Transactions on Wireless Communications*, 2020.
- [7] K. Roth, H. Pirzadeh, A. L. Swindlehurst, and J. A. Nossek, “A comparison of hybrid beamforming and digital beamforming with low-resolution ADCs for multiple users and imperfect CSI,” *IEEE Journal of Selected Topics in Signal Processing*, 2018.
- [8] 3GPP, “Study on channel model for frequencies from 0.5 to 100 ghz,” 3rd Generation Partnership Project (3GPP), Technical report (TR) 38.901, 2022, version 17.0.0.
- [9] A. K. Gupta and J. F. Buckwalter, “Linearity considerations for low-EVM, millimeter-wave direct-conversion modulators,” *IEEE Transactions on Microwave Theory and Techniques*, 2012.
- [10] A. K. Fletcher, S. Rangan, V. K. Goyal, and K. Ramchandran, “Robust predictive quantization: Analysis and design via convex optimization,” *IEEE Journal of Selected Topics in Signal Processing*, vol. 1, no. 4, pp. 618–632, 2007.
- [11] O. Orhan, E. Erkip, and S. Rangan, “Low power analog-to-digital conversion in millimeter wave systems: Impact of resolution and bandwidth on performance,” in *2015 Information Theory and Applications Workshop (ITA)*, 2015, pp. 191–198.
- [12] F. Pasic, M. Hofer, M. Mussbah, S. Sangodoyin, S. Caban, S. Schwarz, T. Zemen, M. Rupp, A. F. Molisch, and C. F. Mecklenbräuker, “Millimeter wave MIMO channel estimation using sub-6 GHz out-of-band information,” *IEEE Transactions on Communications*, 2024, submitted. [Online]. Available: <https://owncloud.tuwien.ac.at/index.php/s/3YP9Uq4Dxx17HeZ>
- [13] J. Lee, G.-T. Gil, and Y. H. Lee, “Channel estimation via orthogonal matching pursuit for hybrid MIMO systems in millimeter wave communications,” *IEEE Transactions on Communications*, vol. 64, no. 6, pp. 2370–2386, 2016.
- [14] B.-W. Min and G. M. Rebeiz, “Ka-band SiGe HBT low noise amplifier design for simultaneous noise and input power matching,” *IEEE Microwave and Wireless Components Letters*, vol. 17, no. 12, pp. 891–893, 2007.